Short- and long-range order in iron and cobalt disilicides thin films investigated by the diffraction anomalous fine structure technique

O. Ersen* and V. Pierron-Bohnes
Institut de Physique et Chimie des Matériaux de Strasbourg, Groupe d'Etude des Matériaux Métalliques (UMR CNRS-46), Université Louis Pasteur, 23 rue du Loess, F-67037 Strasbourg, France

M.-H. Tuilier,† C. Pirri, and L. Khouchaf‡
Laboratoire de Physique et de Spectroscopie Electronique (UMR CNRS-7014), Faculté des Sciences et Techniques, 4 rue des Frères Lumière, F-68093 Mulhouse, France

M. Gailhanou
Laboratoire pour l'Utilisation du Rayonnement Electromagnétique, Centre Universitaire Paris-Sud (CNRS, MEN, CEA), Bâtiment 209 D, F-91198 Orsay, France

(Received 4 September 2002; revised manuscript received 4 December 2002; published 31 March 2003)

The diffraction anomalous fine-structure technique is applied to the characterization of the local order around metallic atoms located in binary and ternary iron and cobalt disilicides thin films prepared by molecular-beam epitaxy on Si(111). The study is first performed on binary compounds, namely, cubic $CoSi_2$ (CaF_2 type), and metastable tetragonal $FeSi_2$ (α-$FeSi_2$-derived type). With the crystallographic structure of both phases known, the first-order data analysis proposed by Proietti *et al.* [Phys. Rev. **59**, 5479 (1999)] is used to reduce the experimental data. The analysis of the Co *K*-edge fine structure collected on the $11\bar{1}$ fundamental diffraction peak of the standard $CoSi_2$ allows the determination of the short-range order around the unique metallic site, in the same way as extended x-ray-absorption fine structure. In addition, it is shown that recording the Fe *K*-edge oscillations on a single superstructure peak of iron disilicide can provide further information about the long-range order in the α-$FeSi_2$-derived-type structure. The value of the long-range-order η parameter is found to be 0.9 ± 0.05. Finally, the method is applied to an epitaxial layer grown at room temperature with the ratio Fe:Si of 0.7:2 and Co:Si of 0.3:2 Si on Si(111) and annealed at 930 K. The analysis of Fe and Co *K*-edge fine structure collected on the $11\bar{1}$ diffraction peak permits to differentiate between Co and Fe local environments in ternary $Co_{0.6}Fe_{0.4}Si_2$ grains having a CaF_2-type structure. These nanostructures are embedded in a $Co_{0.05}Fe_{0.95}Si_2$ matrix whose tetragonal lattice is very close to the α-$FeSi_2$-derived one. The value of the η parameter derived from the analysis of the Fe *K*-edge oscillations on the 001 superstructure peak is found to be 0.8 ± 0.05.

DOI: 10.1103/PhysRevB.67.094116 PACS number(s): 78.70.Ck, 78.70.Dm, 68.55.−a, 81.15.Hi

I. INTRODUCTION

The x-ray-absorption fine-structure (XAFS) technique is a powerful tool to investigate the local distortions around atoms in complex crystalline materials. The interpretation of the modulation of the absorption coefficient above an absorption edge, which is related to the interference between the photoelectron wave function and its scattered part by the neighbor atoms, is now well established.[1,2] However, this technique does not allow an easy separation of the contributions of atoms occupying different sites in a crystalline lattice, since the available information is averaged over all atoms of the same species in the sample. In addition, in the case of mixed phases in the same sample, it is impossible to isolate the contributions of atoms belonging to each of them.

For ten years, the technique of x-ray-diffraction anomalous fine structure[3] (DAFS) has been able to overcome these problems by using the diffraction conditions to select a subset of resonant atoms. DAFS consists of measuring the intensity variation of diffraction peaks as a function of energy at and above an absorption edge of the atoms of interest. The information contained in absorption spectra can also be extracted from energy-dependent diffraction measurements due to the causal relationship between the real and imaginary parts of the atomic scattering amplitude. Consequently, the oscillatory structure in a DAFS spectrum contains at least as much local structural information as XAFS. But, the advantage of DAFS spectroscopy is the ability to combine the chemical and short-range structural sensitivity of x-ray absorption with the long-range structural selectivity of x-ray diffraction (XRD) and, consequently, to provide selective structural information by choosing Bragg peaks separated in the reciprocal space. Due to this crystallographic selectivity, DAFS can be used when analysis by XAFS is difficult or impossible, for example, when isolating local structure about a unique site[4,5] (site selectivity) or separating the contribution of each component in a mixed phase[4] (spatial selectivity). Also, the use of DAFS can overcome the problem of materials containing atoms with absorption edges closely spaced in energy.[6]

The DAFS technique has recently provided great improvements in the study of local distortions induced by the coherent growth of strained nanometric films on a single-crystalline substrate.[7] Nevertheless, from our knowledge, no

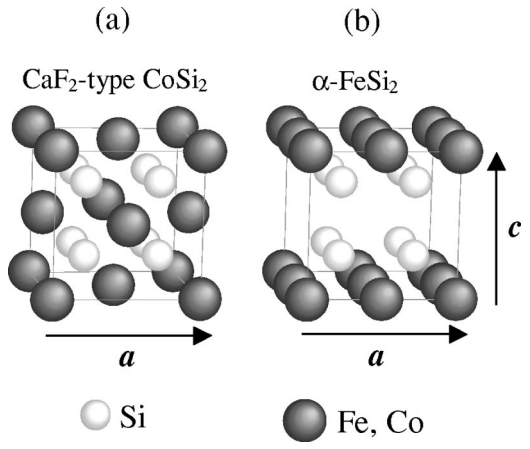

FIG. 1. Structures of the (a) CaF_2-type face-centered-cubic ($CoSi_2$) and (b) tetragonal α-$FeSi_2$ phases.

DAFS investigation of standard compounds grown in thin films has been reported until now. A complete DAFS study performed on thin films of binary compounds whose structure is well known is now of a fundamental interest for a better understanding of the advantage of DAFS with respect to the XAFS technique. The samples we studied are transition-metal disilicide thin films co-deposited by molecular-beam epitaxy (MBE) on a Si(111) substrate at room temperature and annealed above 900 K. For about ten years, new iron and cobalt silicide phases stabilized by the strain induced by epitaxy on Si(111) substrates have been identified, by using either transmission-electron microscopy,[8,9] XRD,[10–12] or extended x-ray-absorption fine structure (EXAFS).[13–15] In this work, we are interested in the ordered disilicide phases that are prepared in thin films by codepositing at room temperature on Si(111)—or previously by solid phase epitaxy (SPE)—and annealing at temperatures as high as 900 K. $CoSi_2$ grown in these conditions crystallizes in the common fluorite (CaF_2) cubic structure represented in Fig. 1(a). Co atoms form a cubic face centered lattice and Si atoms are located in the eight $(\frac{1}{4},\frac{1}{4},\frac{1}{4})$ positions. $FeSi_2$ disilicide has the so-called α-$FeSi_2$-derived tetragonal structure[11] instead. The various structures of the Fe metastable disilicides are well described in the paper of Whiteaker *et al.*[12] Before annealing, the as-deposited thin iron disilicide film ($<$100-Å thick) has the CsCl-derived structure that can be viewed as a disordered version of the CaF_2-type structure: the metallic atoms are randomly distributed into the fcc lattice positions and additional eightfold sites between the Si atoms, at the center of the cube with a unit cell of half the size. Upon annealing this silicide, a depletion of the interstitial sites occurs, which is accompanied by a change in the lattice symmetry, with a reduction of the lattice parameter c along the [001] direction. A layout of the lattice is observed, without reaching the perfect order of bulk α-$FeSi_2$ represented in Fig. 1(b), where one metallic plane (001) out of two is empty. The $FeSi_2$ thin films, then have, after subsequent annealing, a α-$FeSi_2$-derived tetragonal structure. The presence of a small part of iron atoms in the interstitial sites of the lattice gives rise to additional superstructure lines, due to the doubling of the elementary cell. The intensity of the superstructure lines is then related to the occupation factors of the metallic interstitial sites.[11,12] The structural information derived from XAFS experiments has also greatly contributed to accounting for the atomic structure of these novel phases of iron silicides.[14,15] The local order around metallic atoms in CaF_2-type and α-$FeSi_2$-derived phases have indeed their own EXAFS fingerprints. In both, the metallic atoms have 8 Si nearest neighbors, but in a $CoSi_2$ perfect CaF_2 structure, Co atoms have 12 Co next-nearest neighbors (NNN) at $a\sqrt{2}/2$, with a the lattice parameter ($a=5.367$ Å). In contrast, in the bulk α-$FeSi_2$ structure, Fe has 4 Fe NNN located at $a'=2.695$ Å, with a' the in-plane (001) lattice parameter. Considering the results of XRD and EXAFS, it seems wise to record DAFS oscillations on two diffraction lines characteristic of the CaF_2 and tetragonal lattices for a DAFS analysis of $CoSi_2$ and α-$FeSi_2$, respectively. The $11\bar{1}$ fundamental diffraction peak of $CoSi_2$ and the 001 superstructure peak of α-$FeSi_2$ have been chosen for this preliminary study. Particular attention is paid to the treatment of the spectra recorded on the 001 superstructure peak characteristic of the α-$FeSi_2$-type phase. It will be shown that information about long-range order in this partially ordered phase can be obtained from DAFS recorded on a single superstructure peak, as far as interatomic distances and coordination numbers are accurately determined by this technique.

Despite a great deal of effort over the last ten years, attempts to stabilize thin films of iron disilicide in a CaF_2-type lattice have failed. However, way to reach this goal was attempted by preparating by MBE ternary silicides in various compositions.[16] It has been pointed out that the Co and Fe silicides crystallize either in a single or multiple phases, depending on the growth conditions and nominal composition.[17,18] In this work, we present a DAFS analysis of the ternary silicide (TS) formed when Fe and Si are grown with the ratio Fe:Si of 0.7:2 and Co:Si of 0.3:2 on Si(111). The as-deposited TS has the CsCl cubic structure. High-resolution transmission-electronic microscopy (HRTEM) and XRD experiments performed on this TS after annealing at 925 K have revealed a phase separation into grains of the two binary structures described above.[17,18] Both techniques have shown the presence in this film of these two (and only two) phases in equivalent proportions.

The results of this study have been briefly presented in a previous paper (Ref. 22). The aim of the present paper is to describe in detail the treatment of the DAFS spectra recorded at the Fe and Co K edge on the $11\bar{1}$ and 001 peaks belonging to CaF_2-type and α tetragonal phases. A comparison between DAFS and XAFS spectra of the films of standard binary compounds and TSs is emphasized. With the iron atoms present in substantial amounts in both phases of the latter, the analysis of the two sets of Fe K-edge DAFS data allows the characterization of the local environment of Fe in each of them, while Fe K-edge EXAFS data recorded from the same sample should be a mixing of the two.

The paper is organized in the following manner: (i) the first-order DAFS analysis proposed by Proietti *et al.*[19] used as a starting point of this work is summarized in Sec. II; (ii)

the experiments are described in Sec. III; (iii) the data analysis and results of XAFS and DAFS experiments are described in detail in Sec. IV. An accurate normalization of the DAFS data by using the theoretical structure factor values is presented. The DAFS analysis of the partially ordered tetragonal phase in terms of a long-range-order parameter is described in detail. Section V consists of a discussion of the results: though our primary goal was the structural characterization of mixed phases, the last part of the discussion is focused on the advantages of the DAFS technique in the structure determination of partially ordered materials.

II. FIRST-ORDER DAFS ANALYSIS

When analyzing the DAFS spectra, two situations can be encountered.[19] In the first case, only one anomalous site contributes to the diffracted intensity. Then f' and f'' (the ''bare'' atom anomalous corrections to the Thomson atomic scattering factor) can be isolated from the DAFS intensity by an iterative Kramers-Kronig algorithm, without knowing the crystallographic structure, and structural information can be obtained from f'' using standard XAFS analysis methods. In the second case, there are several anomalous crystallographic sites, with different weights. In that case, precise knowledge of the structure is required in order to obtain approximate values of the atomic scattering factors. In this way, an accurate extraction of the DAFS signal is achieved. The data are then analyzed similarly to EXAFS spectra to provide local structural information about each anomalous site.

In our case, the presence of two anomalous sites in the α tetragonal phase renders impossible the use of the iterative integral algorithm. Moreover, the iterative Kramers-Kronig extraction can cause additional errors related to the quality of the data and the theoretical functions used.[20] Consequently, the crystallographic structure factors are calculated using the Thompson atomic scattering factors and the ''bare'' corrections for all atoms. The multiple-anomalous-site method is applied to analyze the DAFS oscillations in order to obtain the structural information in both phases.

In the forward-scattering limit, the atomic scattering factor of an atom A on site j can be written as

$$f_{Aj}(\vec{Q},E)=f_{0A}(\vec{Q})+f'_{0A}(E)+i\cdot f''_{0A}(E)+\Delta f''_{0A}(E)\cdot[\chi'_{Aj}(E)+i\cdot\chi''_{Aj}(E)], \quad (1)$$

where f_{0A} is the Thompson scattering, f'_{0A} and f''_{0A} are the ''bare'' atom anomalous corrections to f_{0A}, and $\Delta f''_{0A}$ is the contribution of the ''bare'' atom resonant electronic transition [the difference between $f''(E)$ and its extrapolation above the edge of its part below the edge]. $\vec{Q}$ is the scattering vector, E is the energy of the incident beam, and $\chi'_{Aj}+i\cdot\chi''_{Aj}$ is the complex fine-structure contribution, which is the correction to the scattering factor due to the local atomic environment of the anomalous atom. The total structure factor is the sum of these atomic contributions:

$$F(\vec{Q},E)=F_0e^{i\phi_0}+\Delta f''_{0A}(E)\cdot\sum_j|\alpha_{Aj}(\vec{Q})|\cdot e^{i\phi_{Aj}}\times[\chi'_{Aj}(E)+i\cdot\chi''_{Aj}(E)], \quad (2)$$

where F_0 is the complex structure factor and ϕ_0 its phase, $\alpha_{Aj}(\vec{Q})=c_{Aj}\cdot e^{-M_{Aj}Q^2}\cdot e^{i\vec{Q}\vec{r}_j}$. c_{Aj} is the occupation factor of atom A on site j, and $e^{-M_{Aj}Q^2}$ the crystallographic Debye-Waller factor. F is thus split into a smooth part (first term) and a oscillatory part (second term).

Neglecting the second-order terms, the first-order DAFS oscillations $\chi_Q(E)$ for a given scattering vector $\vec{Q}$ can be extracted directly from the experimental spectrum and normalized according to the following formula:

$$\chi_Q(E)=\sum_{j=1}^{N_A}w_{Aj}\cdot[\cos(\phi_0-\phi_{Aj})\cdot\chi'_{Aj}+\sin(\phi_0-\phi_{Aj})\cdot\chi''_{Aj}]=\frac{|F_0|}{2\cdot|\alpha_A|\cdot\Delta f''_{0A}}\cdot\frac{I_{DAFS}-I_0}{I_0}, \quad (3)$$

where I_{DAFS} is the experimental intensity corrected for fluorescence background and the absorption of the incident and diffracted beams, I_0 is the smooth curve of the experimental DAFS spectrum, N_A is the number of anomalous atoms, and $w_{Aj}=|\alpha_{Aj}|/|\alpha_A|$. The DAFS normalization factor $S_D=|F_0|/(2\cdot|\alpha_A|\cdot\Delta f''_{0A})$ may be calculated from the crystallographic structure.

The DAFS oscillations can be written in an expression very similar to the EXAFS one:

$$\chi_Q(\vec{k})=\sum_{j=1}^{N_A}\sum_{\Gamma}w_{Aj}(\vec{Q})\cdot amp^{\Gamma}_{Aj}(\vec{k})\cdot\sin\left[2\cdot k\cdot R^{\Gamma}_{Aj}+\delta^{\Gamma}_{Aj}(\vec{k})+\phi_0(\vec{Q},\vec{k})-\phi_{Aj}(\vec{Q})-\frac{\pi}{2}\right], \quad (4)$$

where Γ is a photoelectron-scattering path, $amp^{\Gamma}_{Aj}(\vec{k})$ is the amplitude of the photoelectron scattering, δ^{Γ}_{Aj} the phase shift, and R^{Γ}_{Aj} the effective path length. This equation shows that the DAFS oscillations can be treated as EXAFS data, if the crystallographic weights w_{Aj} and the phases $\phi_0-\phi_{Aj}$, to be added to the photoelectron phase shifts, can be calculated from the crystallographic structure.

III. EXPERIMENT

The epitaxial silicides were prepared on Si(111) in a UHV chamber, with a base pressure of $\sim10^{-10}$ mbar. Prior to loading into the preparation chamber, the Si(111) wafers were cleaned in an ultrasonic bath of ethanol for 30 min and dried in flowing N_2 gas. In order to remove surface oxides and other contaminants, the substrates were first heated at a temperature below 675 K for a few hours and then flashed to 1225 K with residual pressure kept below $\sim5\times10^{-10}$ mbar during the whole process. In this way, we obtained contaminant-free surfaces with sharp (7×7) low-energy electron-diffraction (LEED) patterns. Si, Fe, and/or

Co were evaporated in the 1–2-Å/min range using stable homemade effusion cells. Stoichiometric fluxes of different elements were carefully controlled by a two-quartz-microbalance system. The epitaxial TS was prepared as follows: a 10-Å-thick $Co_{1-x}Fe_xSi_2$ template layer was first grown at room temperature (RT) and subsequently annealed at 823 K. Then a thicker (about 100 Å) $Co_{1-x}Fe_xSi_2$ film was deposited at RT and subsequently annealed at 925 K for one hour. These layers were then capped by an amorphous Si layer to protect them in air. Epitaxy was checked *in situ* with LEED after room-temperature deposition and after annealing at 950 K. In both cases, the LEED pattern exhibited sharp diffraction spots.

EXAFS spectra were collected on the XAS2 beamline at the DCI-Laboratoire pour l'Utilisation du Rayonnement Electromagnétique (LURE) synchrotron-radiation facility, using a Si(111) two-crystal monochromator. The data were recorded at the Fe and Co *K* edges in grazing incidence, the electric vector of the incident beam being nearly parallel (6°) to the surface of the Si(111) substrate. The fluorescence intensity was measured by a seven-element Ge detector. The energy resolution was sufficient to eliminate the fluorescence of Fe atoms above the Co *K* edge. The accumulation lasted about 40 s with 0.2-eV steps. The samples were cooled to about 20 K during the measurements.

The DAFS experiments were carried out on the H10 beamline at DCI-LURE.[21] This beamline is dedicated to material studies, combining x-ray scattering and x-ray-absorption measurements. The white x-ray beam is monochromatized by a two-crystal spectrometer, equipped with Si(111) single crystals. Two mirrors are used to reject harmonics. The monochromatic beam is focused in the vertical and horizontal planes on the sample, that is located at the center of a four-circle goniometer. The focused spot dimension was around 0.5 mm in the scattering plane and 3 mm in the perpendicular direction because of the DCI large source size. Entrance slits were used mainly to clean the beam, which was monitored simultaneously by an ionization chamber and a photodiode measuring the scattering by a Kapton foil situated between the entrance slits and the sample. Two pairs of slits (aperture close to 8 mm$\times$8 mm), separated by a 250-mm pipe under vacuum, were positioned in front of the detector.

The DAFS spectra were recorded in a top-DAFS scan mode, i.e., measuring the maximum intensity of the Bragg reflection as a function of energy. The stability of the beamline and the precise determination of the diffractometer angles at each energy in order to maintain the Bragg conditions achieved a satisfactory signal-to-noise ratio. The fluorescence background was recorded by repeating the DAFS scan after rotating the sample within its plane to an off-peak position. The diffraction and background spectra were recorded with a NaI scintillator or a Si P-Instrinsic-N semiconductor photodiode. Fluorescence XAFS was measured simultaneously using a Si:Li cooled photodiode (resolution 220 eV), placed normally to the incident beam at the sample position in order to decrease the elastic-scattering contribution that could saturate the detector.

The DAFS experiments ran within the 7000–8500-eV energy range with 2-eV energy steps and 10–20-s measuring times depending on the reflected intensity. The polarization vector of the incident beam was normal to the scattering plane. To separate the contribution from each phase, we considered the 001 superstructure diffraction peak for the α tetragonal phase and the $11\bar{1}$ diffraction peak for the CaF_2-type phase, respectively.

IV. DATA ANALYSIS AND RESULTS

As pointed out in introduction, one of purposes of this work was to point out the advantage of DAFS that combines XRD and XAFS techniques. The previous work on XAFS of Co and Fe silicides has provided a clear identification of the local environment of metallic atoms in binary silicid,es and it is interesting to first probe the DAFS technique on binary silicides in comparison with XAFS.

At a nominal $x=0.7$ silicide composition, previous XRD and HRTEM experiments revealed the presence of cubic CaF_2-type and α tetragonal structures approximately in equal proportion in the epitaxial TS film.[17,18] Two well-distinguished types of crystallites are associated with the two silicide structures. The grains have a lateral size of a few tenths of a nanometer, depending on the terrace width (for more details on a HRTEM investigation, see Ref. 22). Our aim was to determine the chemical composition of the two types of crystallites and the local order around Fe and Co atoms in each of them.

Before describing the DAFS data analysis, we first present a quick comparison between EXAFS data recorded at Co and Fe *K* edges of the TS and binary epitaxial $CoSi_2$ and $FeSi_2$, respectively. It will thus become obvious that DAFS is a powerful tool for overcoming the averaging problem occurring in XAFS spectra of multiphased materials.

A. EXAFS

1. EXAFS data reduction

The fluorescence spectra from each of the seven elements of the detector were carefully examined before they were summed. The χ EXAFS signal was extracted following the conventional procedure.[23] After conversion into *k* space, the $\chi(k)$ signals were k^2 weighted and Fourier transformed to between 3.2 and 13.4 $Å^{-1}$. The *R*-space data were Fourier filtered between 1.1 and 2.8 Å and the amplitude was calculated in order to detect the presence of a beat node and determine its position.

2. Co K-edge EXAFS of $CoSi_2$ and the ternary silicide

The EXAFS of $CoSi_2$ grown epitaxially on Si(111) has been studied in detail.[15] The Co *K*-edge EXAFS signals of the TS and binary $CoSi_2$ are compared in Figs. 2(c) and 2(d). The curves present similar shapes with a damping of high-frequency oscillations for the latter, which indicates changes in the distribution of far-distant neighbors. The corresponding Fourier transforms (FT) are shown in Figs. 3(c) and 3(d). The nearest-neighbor (NN) peak in the FT of $CoSi_2$ is quite symmetrical while that of the TS presents a small shoulder

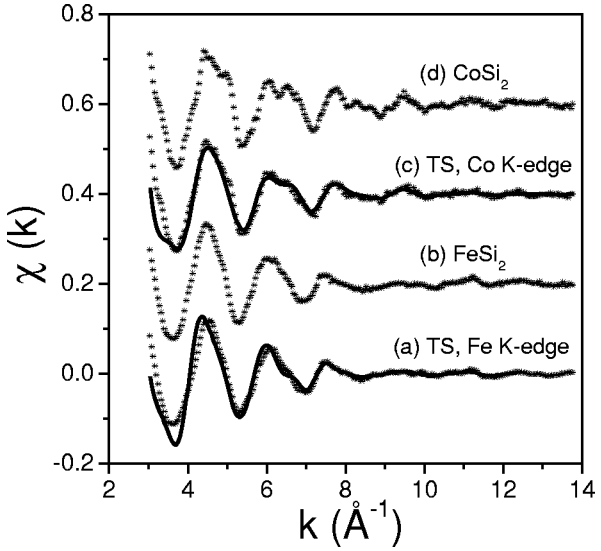

FIG. 2. EXAFS data at 20 K for ternary silicides: (a) Fe *K* edge and (c) Co *K* edge; binary silicides: (b) α-$FeSi_2$ and (d) $CoSi_2$; crosses represent the experiment, the full line the calculation.

on the side of the long distances. The more striking feature in the FT of the TS spectrum is the collapse of the peak located around 3 Å, which is assigned to the 12 Co next-nearest neighbors (NNN) of Co at 3.84 Å in $CoSi_2$. The amplitude envelope of its Fourier filtered contribution underwent a constant reduction by a factor of about 2 over the whole *k* range, that suggests a significant drop in the coordination number of metallic neighbors of Co in the TS with respect to binary $CoSi_2$. At this stage no model was found for fitting the Co *K*-edge XAFS spectrum of the TS. The theoretical EXAFS curves (full lines in Figs. 2 and 3) are outlined in Sec. V.

3. Fe K-edge EXAFS of $FeSi_2$ and the ternary silicide

The Fe *K*-edge EXAFS spectra of the TS and α-$FeSi_2$ and their corresponding FT are shown in Figs. 2 and 3 [curves (a) and (b)], respectively. The data are very similar and only slight differences can be observed in the FT. In epitaxial binary α-$FeSi_2$, Fe is surrounded by eight Si at 2.36 Å and four Fe at 2.70 Å. Whereas the main oscillation in the Co *K*-edge $\chi(k)$ curve of $CoSi_2$ decreases smoothly versus *k*, the Fe *K*-edge spectra of α-$FeSi_2$ and the TS present at about 9 $Å^{-1}$ a beat node which is typical of Fe-Si and Fe-Fe nearby distances.[14] Consequently, the peak located between 1.1 and 2.8 Å splits into two components. The second component is slightly smaller in the TS than in the reference. On the other hand, the lack of peak beyond 3 Å in the FT was attributed to the distortion of the cubic lattice. More details about Fe *K*-edge EXAFS investigation of Fe silicide thin films are given in Ref. 14.

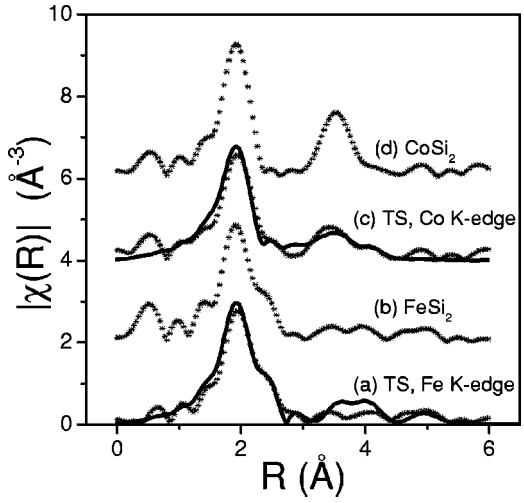

FIG. 3. FT of the k^2-weighted EXAFS data of Fig. 2; ternary silicides: (a) Fe *K* edge and (c) Co *K* edge; binary silicides: (b) α-$FeSi_2$ and (d) $CoSi_2$; crosses represent the experiment, the full line the calculation.

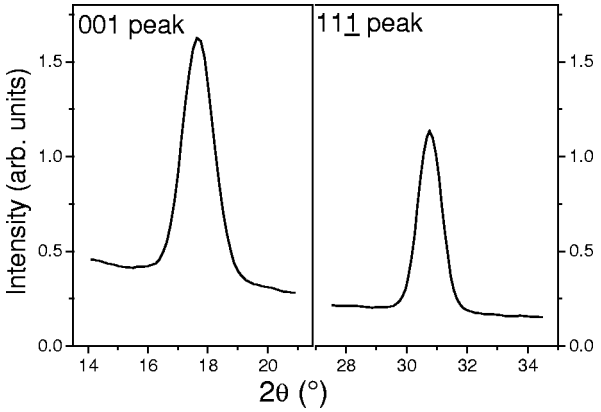

FIG. 4. Normalized intensity of the 001 diffraction peak (α tetragonal phase of the TS) and of the $11\bar{1}$ diffraction peak (CaF_2-type phase of the TS) recorded at 7.5 keV.

In summary, the Fe *K*-edge EXAFS data of TS reveal only a slight decrease of the contribution of Fe atoms at 2.7 Å with respect to α-$FeSi_2$. In contrast, the Co *K*-edge data exhibit strong changes in the distribution of the metallic neighbors at 3.8 Å with respect to the standard binary compound.

B. DAFS

1. DAFS data analysis

Figure 4 shows the results of the $\theta/2\theta$ scan taken at the photon energy of 7.5 keV in the regions the 001 diffraction peak of the α tetragonal phase and of the $11\bar{1}$ diffraction peak of the CaF_2-type cubic phase. The raw DAFS spectra were collected at the top of these peaks at and above Fe and Co *K* edges by measuring the diffracted intensities I_{DAFS} versus the photon energy. Typical DAFS spectra are shown in Fig. 5 (full line). They are corrected for the fluorescence background, by removing the spectra recorded in an off-peak position. Curves (a) and (b) correspond to the 001 superstructure (α tetragonal phase of the TS) and $11\bar{1}$ (CaF_2-type phase of the TS) peaks, respectively. No self-absorption correction was applied since the film thickness was less than 5% of the absorption length.

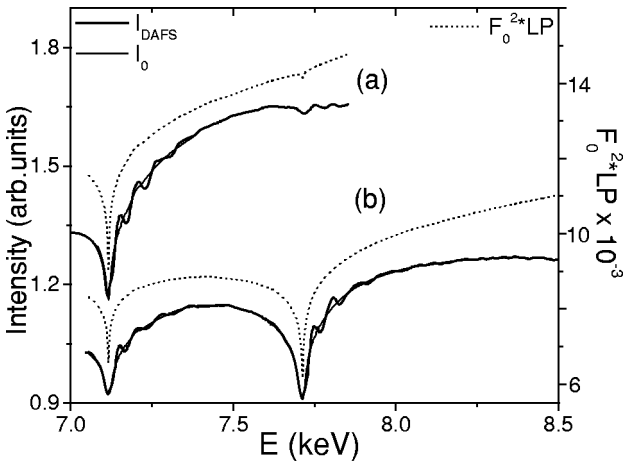

FIG. 5. Raw DAFS spectra recorded at the Fe and Co K edges from the ternary silicide for the (a) tetragonal α-$FeSi_2$ and (b) (I_{DAFS}, full lines) CaF_2-type phases; ($LP\cdot F_0^2$, dashed lines) square of the smooth structure factor F_0^2, corrected for the Lorentz-irradiated area-polarization effects; (I_0, thin lines) calculated smooth parts of the diffracted intensities.

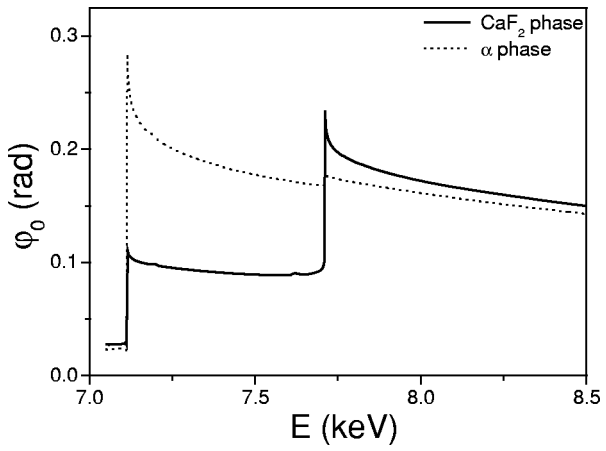

FIG. 6. Theoretical phases (ϕ_0) of the complex structure factors (F_0) for the (dots) tetragonal α-$FeSi_2$ and (full line) CaF_2-type phases. $\Delta\phi=\phi_0-\phi_{Aj}$ are added to the scattering phase shifts calculated by FEFF6 (see text).

The quantitative DAFS analysis started with the calculation of I_0, the smoothing curve (without the fine structure) of the spectra. Generally, after the absorption correction, the intensity of a diffraction peak is proportional to the squared modulus of the structure factor times several terms: the Lorentz-irradiated area-polarization correction term (LP), the detector efficiency (D), and the scale factor (S):

$$I(E)=S\cdot D(E)\cdot LP\cdot F_0^2. \tag{5}$$

To evaluate the complex smooth structure factors F_0 for the two phases, their chemical compositions are required. Thus, the Fe (and Co) amount in each phase is roughly estimated from the Fe (Co) K-edge hollows observed on the spectra of the α tetragonal and CaF_2-type cubic phases. On the other hand, tabulated values are used for the Thompson scattering terms f_0.[24] The values of the anomalous dispersion and absorption corrections, namely, $f_0'(E)$ and $f_0''(E)$, are calculated by using FPRIME program, developed by Cromer and Libermann.[25] The squared modulus of structure factors multiplied by the LP correction ($LP\cdot F_0^2$) are shown in Fig. 5 (dashed line) for the CaF_2-type and tetragonal α-$FeSi_2$ structures, respectively. In order to superpose these terms to the raw spectra, we considered a polynomial function which contains the detector response D and the scale factor S. The best fit of this function gives the smoothed curve I_0 of the spectra (thin line in Fig. 5).

The DAFS oscillations are extracted from the raw data and normalized according to formula (3). Taking advantage of the knowledge of the crystallographic structures, the coefficients $|F_0|$, $|\alpha_A|$, and $\Delta f_{0A}''$ are calculated for the reference compounds ($CoSi_2$ and $FeSi_2$) and the TS, at Co and Fe K edges. The relevant DAFS oscillations obtained in this way are now treated as EXAFS oscillations by using formula (4). The crystallographic weights w_{Aj} are expressed as functions of occupation factors c_i of the metallic sites, and the phase shifts $\Delta\phi_j=\phi_0-\phi_{Aj}$ are calculated from the crystallographic structure in each phase. Figure 6 shows ϕ_0 at the Fe and Co K edges as a function of the wave vector of the photoelectron. Let us mention that, at a given edge, the assumption that $\Delta\phi_j$ is constant over the whole spectrum is not true because the anomalous contribution to F_0 smoothly changes as a function of energy. These variations result from the fact that Fe and Co atoms are close to each other in the Periodic Table, their K edges being only 0.6-keV separated.

We analyzed the DAFS oscillations using the FEFFIT program.[26] FEFFIT performs the fit to the data in R or k space using calculated path contributions from FEFF6 (Ref. 27) as scattering theoretical standards. One of the substantial advantages of this program is that it includes multiple-scattering (MS) calculations and consequently it uses an analysis procedure based on a sum over scattering paths (as opposed to ''shells''), with no distinction between single- and multiple-scattering paths. The standard XAFS parameters to be varied to find the best fit of the data are characteristic of each scattering path. Moreover, by using the FEFFIT program, we can build sophisticated models taking into account relations between the fitting parameters.

We include in FEFFIT calculations contributions from the first three single-scattering shells as well as several multiple-scattering paths involving either two nearest-neighbor Si atoms or a nearest-neighbor Si and a second-nearest-neighbor metal atom. Generally, MS paths have lower contributions to the total signal than the single-scattering (SS) ones due to the higher values of their Debye-Waller (DW) factors. Nevertheless, we considered all MS paths whose FEFF6 calculated scattering mean amplitude (defined as the integral of the scattering amplitude over the full energy range) exceeds 7% of the path of largest amplitude.

Figure 7 shows the Fe K-edge DAFS oscillations and best fits of [Fig. 7(a)] the α-$FeSi_2$ binary silicide, [Fig. 7(b)] the α-$FeSi_2$-derived phase in the ternary silicide, and [Fig. 7(c)] the CaF_2-type phase in the ternary silicide. The corresponding FT of the k^2-weighted DAFS data and of the simulations are represented in Fig. 8. The results of the fits are summarized in Table I.

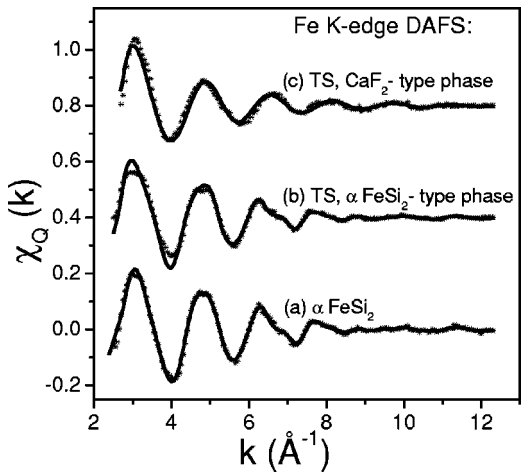

FIG. 7. Comparison of (dots) Fe *K*-edge DAFS oscillations and (full line) best fits using the values of Table I of (a) α-$FeSi_2$-derived binary silicide; (b) α-$FeSi_2$-derived phase in the ternary silicide; (c) CaF_2-type phase in the ternary silicide.

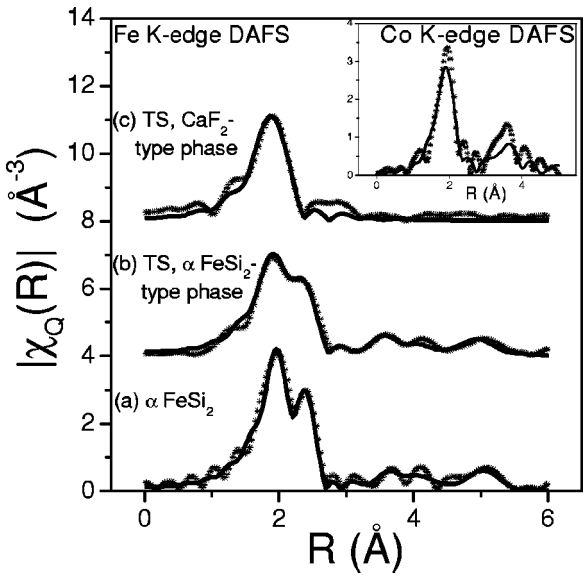

FIG. 8. FT of the k^2-weighted DAFS data presented in Fig. 7: (a) α-$FeSi_2$-derived binary silicide; (b) α-$FeSi_2$-derived phase in the ternary silicide; (c) CaF_2- type phase in the ternary silicide; dots represent experiments, and full lines the simulations. Inset: FT of Co *K*-edge DAFS recorded from (dots) binary $CoSi_2$, and (full line) CaF_2-type phase in the ternary silicide.

2. DAFS data recorded on the 11$\bar{1}$ fundamental peak of the CaF_2-type structure

The Co and Fe *K*-edge DAFS data collected at the top of the 11$\bar{1}$ peak provide selective information on the local order around metallic atoms located in the CaF_2-type lattice. The Fe concentration on the metallic sites of the CaF_2-type phase in the TS is found to be as high as 40%. The nominal composition of the cubic phase is thus close to $Co_{0.6}Fe_{0.4}Si_2$.[22]

Several free parameters are introduced in the FEFFIT simulations in order to describe the local structure of the $CoSi_2$ and $Co_{0.6}Fe_{0.4}Si_2$ (CaF_2). They are the metal-Si nearest-neighbor and metal-metal next-nearest-neighbor distances on one hand, and the mean-square displacements σ^2 (DW factor) for each SS path on the other hand. Considering that each MS path involves several SS paths, the initial values of the DW factors for MS paths are expressed as functions of the DW factors for the relevant SS paths. By fitting the spectra recorded at the Co *K* edge on the 11$\bar{1}$ diffraction peak, we obtained the Co-Si and Co-metal distances and DW factors in the CaF_2-type phases of the binary $CoSi_2$ and TS. In contrast, by fitting the spectrum recorded at the Fe *K* edge on the same peak in the TS, we deduce the Fe-Si and Fe-metal distances and DW factors in this CaF_2 phase. Let us mention that, due to the close atomic numbers of Fe and Co, a separation of the second-shell metal neighbors in Fe and Co subshells is not possible.

The Fe *K*-edge DAFS signal recorded on the 11$\bar{1}$ fundamental peak of $Co_{0.6}Fe_{0.4}Si_2$ (CaF_2) [Fig. 7(c)] presents a regular decrease of amplitude versus *k*, and the NN peak in the FT [Fig. 8(c)] is roughly symmetrical. In the inset of Fig. 8, the Co *K*-edge DAFS data recorded on the 11$\bar{1}$ peak of $CoSi_2$ (crosses) and $Co_{0.6}Fe_{0.4}Si_2$ (CaF_2) (full line) are presented for comparison. The curves are similar, with lower amplitude in the case of $Co_{0.6}Fe_{0.4}Si_2$ (CaF_2). There is a striking similarity between the peaks located between 1.8 and 2.4 Å in the FT of Fe *K*- [Fig. 8(c)] and Co *K*-edge DAFS (inset, Fig. 8, full line) of the TS. They are quite symmetrical, which indicates that Fe and Co have roughly the same NN environment in $Co_{0.6}Fe_{0.4}Si_2$ (CaF_2). The value of the Fe-Si distance is found to be 2.36 Å in $Co_{0.6}Fe_{0.4}Si_2$ (CaF_2) instead of 2.32 Å (Co-Si distance in $CoSi_2$ and the TS). The lack of peak above 3 Å in Fe *K*-edge data of $Co_{0.6}Fe_{0.4}Si_2$ (CaF_2) reveals the existence of stronger local distortions around Fe than Co.

3. Long-range order. DAFS data recorded on the 001 superstructure peak in the α tetragonal phases of the TS and binary $FeSi_2$

A method is now carried out to derive structural information about long-range order (LRO) from DAFS data recorded on superstructure peaks. Its relevance will be emphasized for the classes of ordered materials where LRO is related to the presence of anomalous atoms in two (or more) local environments. Two situations can be encountered: (i) the distances of the resonant atom to its nearest neighbors are different in the two sites; (ii) the environment of the anomalous atoms consists of different neighbor elements, for example, low- and high-*Z* atoms or vacancies in various proportions for the two (or more) sites.

With respect to conventional XRD, which is the usual way of measuring the LRO parameter, our method does not seem to be very easy to carry out. But, in a conventional XRD experiment, this parameter is usually deduced from the intensity ratio of a superstructure peak to a fundamental peak. Consequently, we need an isolated diffraction peak of both types, whereas the same information can be obtained from a DAFS spectrum recorded on a single superstructure peak. In the present work, we are interested in the determination of the LRO parameter in the binary and ternary

TABLE I. Structural parameters derived from the analysis of Fe and Co *K*-edge DAFS spectra recorded on the 001 superstructure peak (α tetragonal phase in the ternary silicide and binary $FeSi_2$) and the $11\bar{1}$ fundamental peak (CaF_2-type phase in the ternary silicide and binary $CoSi_2$).

	Pair	R (Å)	N	σ^2 (Å^2)	η	δ
Binary $FeSi_2$	Fe-Si	2.37(1)	8	0.003(1)	0.9(1)	0.27(1)
(Fe *K* edge)	Fe-Fe	2.70(2)	4	0.004(1)		
TS: α tetragonal	Fe-Si	2.37(1)	8	0.003(1)	0.8(2)	0.27(1)
phase (Fe *K* edge)	Fe-Fe(Co)	2.70(2)	4	0.005(1)		
TS: CaF_2-type	Fe-Si	2.36(1)	8	0.005(1)		
phase (Fe *K* edge)	Fe-Fe(Co)					
TS: CaF_2-type	Co-Si	2.32(1)	8	0.006(1)		
phase (Co *K* edge)	Co-Co(Fe)	3.80(2)	12	0.011(2)		
Binary $CoSi_2$	Co-Si	2.32(1)	8	0.003(1)		
(Co *K* edge)	Co-Co	3.79(2)	12	0.007(1)		

α-$FeSi_2$-type phases by using DAFS. In any case, the LRO study in the TS by classical XRD is not possible because no isolated fundamental peak is available for the α phase: Indeed both CaF_2-type and α tetragonal phases are derived from the same disordered CsCl-type phase, and their fundamental peaks cannot be separated.

We address now the occupation factors of the two Fe sites in the thin Fe silicide films. Unlike the $CoSi_2$-based thin films which are made of a totally ordered cubic CaF_2-type phase, the $FeSi_2$ thin films present a tetragonal structure, with additional sites, characterized by their degree of vacancy.[11,12,14] The DAFS signal recorded on a superstructure peak is sensitive to that partial order through two effects: the occupation factor difference between the two types of metallic (001) planes and the relative positions of the planes in the unit cell.

Moreover, some assumptions can be made in order to improve the fitting procedure. The Co concentration in the metallic sites of the α tetragonal phase of the TS is found to be only about 5%. The nominal composition of this phase is $Co_{0.05}Fe_{0.95}Si_2$, very close to that of the binary $FeSi_2$ compound. Whereas the incorporation of a large amount of Fe in the CaF_2-type lattice induces strong distortions in $Co_{0.6}Fe_{0.4}Si_2$ with respect to binary $CoSi_2$,[22] the tetragonal structure of α-$FeSi_2$ and α-$Co_{0.05}Fe_{0.95}Si_2$ should be similar. Following these considerations, the fitting structural parameters for the α-$FeSi_2$-type phases can be defined in a slightly different way here than in Sec. IV B 2, in order to extract more information about long-range order in α-$FeSi_2$ and α-$Co_{0.05}Fe_{0.95}Si_2$: the lattice parameters are used as variable parameters instead of path lengths, which allows taking into account the MS paths without increasing the number of adjustable parameters.

Before describing the fitting procedure, we explain the meaning of DAFS data collected on superstructure peaks about LRO. The structure of the α-$FeSi_2$ phase observed in the bulk phase diagram at high temperature ($T > 1210$ K)

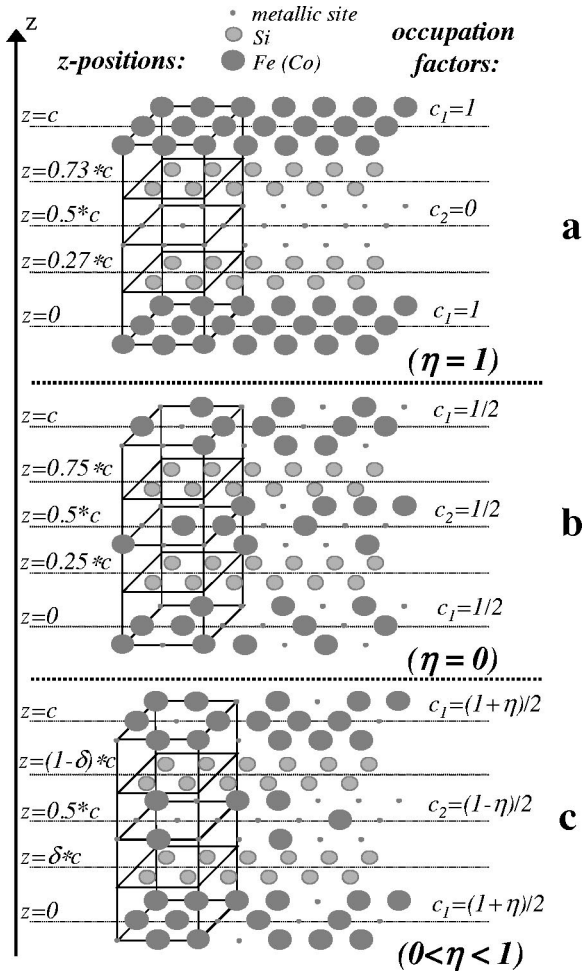

FIG. 9. Schema of the layout of the Fe planes in the binary Fe disilicides: (a) bulk ordered α-$FeSi_2$ phase; (b) disordered CsCl-type $FeSi_2$; (c) partially ordered α-$FeSi_2$-derived phase.

can be described as a stacking of Fe filled and empty (001) planes at $z=0$ and $z=c/2$, respectively, separated by Si planes. A representation of this ordered phase is given in Fig. 9(a). The thin strained epitaxial $FeSi_2$ films crystallize in tetragonal structures, which are disordered or partially ordered, depending on the preparation conditions. Actually, when a binary $FeSi_2$ thin film (<100 Å) is grown epitaxially at room temperature with the ratio Fe:Si of 1:2 on Si(111), its structure can be considered as derived from the cubic CsCl type observed in FeSi silicides grown on Si (111), with vacancies randomly distributed in the Fe planes,[11,12,14] according to the sketch of Fig. 9(b). After annealing this disilicide at 925 K, an ordering of the vacancies is observed: one (001) Fe plane over two is partially emptied and the other plane enriched. An alternate distribution takes place along z axis that can be described as a stacking of partially full and empty (001) Fe planes, alternating with full Si planes [Fig. 9(c)]. To describe this order along the z axis, we can define c_1 and c_2, the occupation factors of the two (001) Fe sublattices. The occupation factors reported by Jedrecy *et al.*[11] for $FeSi_2$ grown epitaxially by solid phas epitaxy (15-Å-thick silicide annealed at 773 K) are about $c_1=\frac{5}{6}$ and $c_2=\frac{1}{6}$. The degree of chemical order can also be described by the long-range-order parameter η defined as $\eta=c_1-c_2$. With this definition of η the maximum of chemical order ($\eta=1$) corresponds to the α-$FeSi_2$ bulk phase ($c_1=1$, $c_2=0$) and its minimum ($\eta=0$) to the CsCl-type phase ($c_1=c_2=0.5$ with a random distribution of the Fe vacancies on both Fe sublattices). Since $c_1+c_2=1$ at any composition, we obtain $c_1=(1+\eta)/2$ and $c_2=(1-\eta)/2$.

On the other hand, the relative z positions of the two Si planes are different in the ordered phase ($0.27\cdot c$ and $0.73\cdot c$ for the α-$FeSi_2$ bulk phase[11]) and in the disordered phase ($0.25\cdot c$ and $0.75\cdot c$ for the CsCl-type phase), where c is the lattice parameter of the tetragonal α phase along the z axis. This structural change can be described by a parameter δ varying between 0.25 and 0.27, defined by the positions of the Si planes at $z=\delta\cdot c$ and at $z=(1-\delta)\cdot c$. Consequently, a precise knowledge of δ (that can be deduced from the Fe-Si and Fe-Fe bond length) provides information on the LRO in the partially ordered α-$FeSi_2$-type phase. The correlation between the values of η and δ will allow to test whether the results are meaningful.

In a diffraction experiment, the spectra must be recorded on the superstructure peaks in order to access LRO. Let us develop the formula of the DAFS oscillations in the case of the 001 superstructure peak. In the elementary cell of the derived α-$FeSi_2$-type phase, there are four metallic sites at $z=0$ with an occupation factor $c_1>0.5$, four metallic sites located in antisite positions at $z=c/2$ with an occupation factor $c_2<0.5$, and eight Si sites in intermediate positions (occupation factor $c_{Si}=1$) at $z=\delta\cdot c$ and $z=(1-\delta)\cdot c$. The structure factor can be written as

$$\begin{aligned} F(\vec{Q},E) &= 4\cdot c_1\cdot f_{M1}+4\cdot c_2\cdot f_{M2}\cdot e^{i\pi}+4\cdot f_{Si}\cdot e^{i2\pi\delta} \\ &\quad +4\cdot f_{Si}\cdot e^{i2\pi(1-\delta)} \\ &= 4\cdot[c_1\cdot f_{M1}-c_2\cdot f_{M2}+2\cdot f_{Si}\cdot\cos(2\pi\cdot\delta)], \end{aligned} \tag{6}$$

where f_{M1} and f_{M2} are the atomic scattering factors of the metal atoms located at $z=0$ and $z=c/2$, and f_{Si} is the atomic scattering factor of the Si atoms. When the DAFS spectrum is recorded at the metal (Co or Fe) K edge, the atomic factors f_{M1} and f_{M2} of the anomalous atoms split into a smooth part and an oscillatory part, according to Eq. (1). Let us note χ_1 and χ_2, the two complex fine-structure factors, which are the corrections to f_{M1} and f_{M2} due to the local atomic environments of anomalous atoms at each position ($z=0$ and $z=c/2$). In the present case, χ_1 and χ_2 are associated with the two different local Fe environments in this phase, i.e., the environments of the atoms located in a Fe-rich plane (at $z=0$) and a Fe-poor plane (at $z=c/2$), respectively. We can also define the average and the difference of complex fine-structure factors, $\bar{\chi}=(\chi_1+\chi_2)/2$ and $\Delta\chi=\chi_1-\chi_2$. The amplitude of $\Delta\chi$ is directly related to the value of η (it becomes 0 when $\eta=0$, and is maximum when $\eta=1$).

According to the formula (3), the modulation of the structure factor (namely, "the DAFS oscillations") can be written as a linear combination of χ_1 and χ_2:

$$\begin{aligned} \chi_{sup} &= c_1\cdot\chi_1-c_2\cdot\chi_2 \\ &= \frac{1+\eta}{2}\cdot\chi_1-\frac{1-\eta}{2}\cdot\chi_2 \\ &= \eta\cdot\bar{\chi}+\frac{1}{2}\cdot\Delta\chi. \end{aligned} \tag{7}$$

This equation highlights the connection between the modulation (χ_{sup}) of the structure factor characteristic of the 001 superstructure peak and LRO along the z axis: for the disordered CsCl-type phase, $c_1=c_2=0.5$, $\chi_1=\chi_2$, and consequently $\chi_{sup}=0$; in contrast, for the bulk ordered α-$FeSi_2$-type phase, $c_1=1$, $c_2=0$, and consequently $\chi_{sup}=\chi_1$.

By analyzing a DAFS spectrum recorded on a superstructure diffraction peak and normalized according to the formula (3), one can obtain information on the order parameter in the partially ordered α-$FeSi_2$-type phase. This information is much less accurate from the EXAFS or DAFS spectra recorded on a fundamental peak: in these cases, the DAFS or EXAFS oscillations can be written as

$$\chi_{fond}=c_1\cdot\chi_1+c_2\cdot\chi_2=\frac{1+\eta}{2}\cdot\chi_1+\frac{1-\eta}{2}\cdot\chi_2=\bar{\chi}+\frac{\eta}{2}\cdot\Delta\chi. \tag{8}$$

If the environments characterized by χ_1 and χ_2 are not very different (i.e., if η and $\Delta\chi$ are near zero and δ is close to 0.25), we obtain $\chi_{fond}\approx\chi_1$ at the second order in η. In contrast, for the spectrum recorded on the 001 peak, the DAFS oscillations always depend on the order parameter, even if χ_1 and χ_2 are not very different:

$$\chi_{sup}=\frac{1+\eta}{2}\cdot\chi_1-\frac{1-\eta}{2}\cdot\chi_2\approx\eta\cdot\chi_1. \tag{9}$$

Consequently, DAFS recorded on the superstructure peak is quite sensitive to the LRO parameter since χ_{sup} depends on

η at the first order. In contrast, the major contribution to DAFS recorded on the fundamental peak χ_{fond} is $\overline{\chi}$. Therefore, χ_{sup} is much more sensitive to η than χ_{fond}.

In order to estimate more accurately δ values for the Si planes in these partially ordered phases, and to correlate them to η, in the simulations we expressed the Fe-Si and Fe-metal distances as functions of δ, a, and c, the lattice parameters. Note that this approach is quite acceptable, because the Co content in the tetragonal phase of the TS is small and the local distortions around Fe atoms are negligible. Moreover, since the vacancies are randomly distributed on the two metallic planes of this structure, the FEFF6-calculated backscattering amplitudes are multiplied by the occupation factors of the metallic sites involved in each scattering path. Furthermore, the relevant DAFS oscillations for these partially ordered tetragonal phases are expressed as a function of two contributions corresponding to the two different atomic environments, according to the formula (7). In this way, the free parameters used in the fits are the lattice parameters a, η, and δ and the DW factors for the single-scattering paths. Note that the lattice parameter c was fixed at the values previously measured by XRD.

The Fe *K*-edge DAFS data collected with reflection 001 [Figs. 7(a) and 7(b) for α-$FeSi_2$ and the TS, respectively] look very similar, with a minimum of the amplitude around 9 $Å^{-1}$, which is typical of close Fe-Si and Fe-Fe distances (see Sec. IV A). The corresponding FT are shown in Fig. 8: the splitting of the NN peak is clearly observed on both curves, less marked on the FT of the TS spectrum [Fig. 8(b)]. In the binary $FeSi_2$ and the tetragonal phase of the TS, the Fe-Si and Fe-Fe distances are found to be 2.37 and 2.70 Å, respectively. The values of the long-range order parameters are given in Table I.

V. DISCUSSION

XRD and HRTEM reveal the presence of two distinct phases in the ternary silicide. Since Fe and Co atoms are not differentiated by these techniques, a quick analysis could conclude a phase separation into two binary compounds, namely, $FeSi_2$ and $CoSi_2$. However, the Co *K*-edge EXAFS data of the TS and $CoSi_2$ (CaF_2) silicide present significant differences. Therefore, this phase separation can be ruled out. It becomes evident that the situation is more complex. The anomalous diffraction reveals the presence of Fe in both phases (40% in the metallic sites of the CaF_2-type phase and 95% in the metallic sites of the α tetragonal phase) that makes impossible the analysis of the local order around Fe atoms from EXAFS measurements.[22] Nevertheless, by recording the DAFS spectra on two different peaks (characteristic of the CaF_2-type and α tetragonal phases), we are able to differentiate the local environment of Fe atoms in each phase.

The discussion is now focused on two main points that have not been extensively treated until now, concerning the contribution of DAFS to the structural study of multiphased and partially ordered materials: First, we recall the advantage of the DAFS technique over XAFS technique in the study of local order in a mixed phase. Secondly, we highlight a more advanced potentiality of DAFS, which appears to be a good technique for providing information on LRO in the classes of materials listed in Sec. IV B 3.

A. Short-range order

The atomic structure of the two phases is more easily understood by the analysis of DAFS oscillations. Let us begin with the analysis of the local order in the metallic sites of the tetragonal phases, namely, α-$FeSi_2$ and α-$Co_{0.05}Fe_{0.95}Si_2$. Their structure should be very similar, because they are grown epitaxially in the same conditions and the Co amount in the tetragonal phase of the TS is only about 5%. This hypothesis is confirmed by the similar forms of the DAFS data and the FT corresponding to both phases (Figs. 7 and 8), as well as the similar values of the NN and next-nearest-neighbor distances derived from the fits of data (Table I). However, the DW parameters of the ternary tetragonal phase are higher than those of the binary $FeSi_2$. Indeed, the iron silicide tetragonal lattice, which is not suited to cobalt silicide, seems to be distorted by the insertion of Co.

The results of the analysis of CaF_2-type phases of the binary $CoSi_2$ and ternary $Co_{0.6}Fe_{0.4}Si_2$ have been described elsewhere.[22] Let us summarize the main features of these phases deduced from the analysis of the DAFS spectra. In $Co_{0.6}Fe_{0.4}Si_2$, either Co or Fe atoms occupy the metallic sites of this CaF_2-type phase. The Co-Si and Fe-Si bond lengths are found to be 2.32 Å and 2.36 Å, respectively. The latter value is close to the Fe-Si bond length in the tetragonal phase (2.37 Å). Nevertheless, Fe and Co atoms are located in equivalent sites, with eightfold coordination in the CaF_2-type lattice, and the significantly larger Fe-Si distances induce lattice distortions. They are revealed in the damping of the Fourier-transformed contribution at about 3.80 Å at both Fe and Co *K* edges with respect to $CoSi_2$, but not in the lattice symmetry.

Moreover, we can now account for EXAFS spectra recorded from the TS (Sec. IV A). Each of them (Fe and Co *K* edges) splits into two DAFS spectra, related to fundamental and superstructure peaks, respectively. The calculated Fe *K*-edge EXAFS curve of the TS and its corresponding FT are presented in Figs. 2(a) and 3(a) (full lines), respectively. They are obtained from a linear combination of three χ'' functions: each of them corresponds to each of the three different sites of Fe atoms (two sites are located in the α tetragonal phase and one in the CaF_2-type phase). These different contributions are calculated by using the FEFF6 program with the structural parameters derived from the analysis of Fe *K*-edge DAFS recorded at both $11\overline{1}$ and 001 peaks. In view of the low concentration of Co in the α tetragonal phase, the Co *K*-edge theoretical EXAFS curve of the TS [Figs. 2(c) and 3(c), full lines) is calculated using the structural parameters derived from the analysis of Co *K*-edge DAFS recorded at the $11\overline{1}$ peak only. We find that DAFS technique, which adds spatial and site selectivity to XAFS, is a powerful approach to investigate the short-range order in nanostructured advanced materials.

B. Long-range order

In Sec. IV B 3, it was shown that DAFS spectra recorded on the 001 superstructure peak of the tetragonal phases are related not only to short-range order around Fe but also to LRO. Such phases are indeed characterized by their η LRO parameter, which is related to the occupation factors of the metallic sites at c with respect to $c/2$. In the binary $FeSi_2$ silicide, we get $\eta=0.9$ (Table I). This value is very close to 1 and corresponds to $c_1=0.95$ and $c_2=0.05$. This new result shows that the ordering in the tetragonal epitaxial disilicide is almost as perfect as that in the bulk equilibrium phase. It also appears to be much more ordered than the layer obtained by Jedrecy *et al.*:[11] these authors showed that $c_1 \approx 0.83$ and $c_2 \approx 0.17$, corresponding to $\eta=0.67$. In the ternary α-$Co_{0.05}Fe_{0.95}Si_2$, the metallic planes contain a small amount of Co atoms, about 5%, as shown from the quantitative anomalous diffraction measurements. The smaller value of the LRO parameter in this phase ($\eta=0.8$) suggests that the Co atoms occupy rather antisite positions (at $z=c/2$). Indeed, in the partially ordered tetragonal phase [Fig. 9(c)], there are two Si-metal interplanar distances, from Si at $\delta \cdot c$ to metallic atoms at $z=0$ on one hand, and metallic atoms at $z=c/2$ on the other hand. The former interplanar distance, equal to $\delta \cdot c$, is slightly longer than the latter, equal to $z=c/2-\delta \cdot c$ ($\delta > 0.25$). In consequence, since the Co-Si distance is usually shorter than that of Fe-Si, the planes at $z=c/2$ better accommodate the location of Co atoms than the planes at $z=0$.

The δ values deduced from the simulations are reported in the last column of Table I. They are roughly equal to 0.27 (the maximum value of δ, corresponding to the totally ordered bulk phase) and consequently in fair agreement with the high value of the η parameters.

The sensitivity of DAFS to LRO could be improved by choosing the x-ray beam polarization perpendicular to the (001) planes, along which full and empty metallic planes alternate with Si planes. Experiments are in progress in order to improve the accuracy of the determination of out-of-plane distances by recording DAFS on Bragg peaks having various spatial orientations.

VI. CONCLUSION

In this study, the chemical order in Co and Fe disilicides is thoroughly investigated in terms of short- and long-range order by using the DAFS technique. Previously, EXAFS was emphasized due to its ability to differentiate between local environments of different atoms, even close in the Periodic Table. The short-range order around Fe and Co in the binary standard compounds is typical of the α-$FeSi_2$ and $CoSi_2$ (CaF_2) phases, respectively. The comparative study of anomalous diffraction at Fe and Co *K* edges on two XRD peaks clearly indicates that both elements are present in the two phases of the ternary silicide film. In such a situation, EXAFS is unable to derive information about interatomic distances and coordination numbers of each element in each phase. The DAFS technique is well suited to separately solve the local structure. Thus, since the iron atoms are present in substantial amounts in both phases of the ternary silicide, the analysis of the two sets of Fe *K*-edge DAFS data allows the characterization of the local environment of Fe in each of them, while Fe *K*-edge EXAFS data recorded from the same sample appear to be a mixing of the two. The use of DAFS permits to take advantage of the selectivity of XRD and to obtain accurate values of the structural parameters.

Beyond this application of the new DAFS synchrotron technique, interesting fundamental conclusions can be derived from this study concerning the connection between the chemical order in a complex material and the XRD superstructure peaks. We have demonstrated that DAFS recorded on a superstructure peak yields information about LRO in classes of materials where LRO is related to several distinct environments of the same element. In the most cases, the measurement of the intensity ratio of the superstructure to the fundamental peak is enough to reach this goal. However this approach has to be considered in mixed phases, when the fundamental peaks of two or several phases are superimposed.

ACKNOWLEDGMENTS

We are grateful to D. Berling for preparing the samples and for his kind help with the synchrotron data collection. We also wish to thank R. Cortès (D21 beamline of the LURE) for providing us with assistance during the EXAFS measurements and D. Thiaudière (H10 beamline of the LURE) for his assistance during the DAFS experiments.

*Corresponding author. Present address: Equipe de Recherche Technologique, Université de Haute Alsace, 61 rue Albert Camus, F-68093 Mulhouse Cedex, France. Electronic address: o.ersen@uha.fr

†Present address: Equipe de Recherche Technologique, Université de Haute Alsace, 61 rue Albert Camus, F-68093 Mulhouse Cedex, France.

‡Present address: Centre de Recherche de l'Ecole des Mines de Douai, 941, rue Charles Bourseul, B.P. 838, 59508 Douai Cedex, France.

[1] See, for example, *X-ray Absorption: Principles, Applications, Techniques of EXAFS, SEXAFS and XANES*, Vol. 92 of *Chemical Analysis*, edited by D. C. Koningsberger and R. Prins (Wiley, New York, 1988).

[2] J. J. Rehr and R. C. Albers, Rev. Mod. Phys. **72**, 621 (2000), and references therein.

[3] H. Stragier, J. O. Cross, J. J. Rehr, L. B. Sorensen, C. E. Bouldin, and J. C. Woicik, Phys. Rev. Lett. **69**, 3064 (1992).

[4] L. Sorensen, J. Cross, M. Newville, B. Ravel, J. Rehr, H. Stragier, C. Bouldin, and J. Woicik, in *Resonant Anomalous X-ray Scattering: Theory and Applications*, edited by G. Materlik, C. Sparks, and K. Fischer (North-Holland, Amsterdam, 1994).

[5] J. Vacínová, J.-L. Hodeau, P. Wolfers, J. P. Lauriat, and E. Elkaïm, J. Synchrotron Radiat. **2**, 236 (1995).

[6] B. Ravel, C. E. Bouldin, H. Renevier, J.-L. Hodeau, and J.-F. Berar, Phys. Rev. B **60**, 778 (1999).
[7] J. C. Woicik, J. O. Cross, C. E. Bouldin, B. Ravel, J. G. Pellegrino, B. Steiner, S. G. Bompadre, L. B. Sorensen, K. E. Miyano, and J. P. Kirkland, Phys. Rev. B **58**, R4215 (1998).
[8] H. von Känel, K. A. Mäder, E. Müller, N. Onda, and H. Sirringhaus, Phys. Rev. B **45**, 13 807 (1992).
[9] H. von Känel, C. Schwarz, S. Goncalves-Conto, and E. Müller, Phys. Rev. Lett. **74**, 1163 (1995).
[10] J. Chevrier, P. Stocker, Le Than Vinh, J. M. Gay, and J. Derrien, Europhys. Lett. **22**, 449 (1993).
[11] N. Jedrecy, A. Waldhauer, M. Sauvage-Simkin, R. Pinchaux, and Y. Zheng, Phys. Rev. B **49**, 4725 (1994).
[12] K. L. Whiteaker, I. K. Robinson, C. Benson, D. M. Smilgies, N. Onda, and H. von Känel, Phys. Rev. B **51**, 9715 (1995).
[13] U. Kafader, M. H. Tuilier, C. Pirri, P. Wetzel, G. Gewinner, D. Bolmont, O. Heckmann, D. Chandesris, and H. Magnan, Europhys. Lett. **22**, 529 (1993).
[14] C. Pirri, M. H. Tuilier, P. Wetzel, S. Hong, D. Bolmont, G. Gewinner, R. Cortès, and H. von Känel, Phys. Rev. B **51**, 2302 (1995).
[15] C. Pirri, S. Hong, M. H. Tuilier, P. Wetzel, G. Gewinner, and R. Cortès, Phys. Rev. B **53**, 1368 (1996).
[16] S. Hong, C. Pirri, P. Wetzel, and G. Gewinner, Phys. Rev. B **55**, 13 040 (1997).
[17] L. Khouchaf, D. Berling, V. Pierron-Bohnes, C. Pirri, S. Hong, P. Wetzel, G. Gewinner, M. H. Tuilier, S. Lefebvre, and R. Cortès, in *Mechanisms and Principles of Epitaxial Growth in Metallic Systems*, edited by L. T. Wille, C. P. Burmester, K. Terakura, G. Comsa, and E. D. Williams, Mater. Res. Soc. Symp. Proc. No. 528 (Materials Research Society, Pittsburgh, 1998), p. 75.
[18] O. Ersen, V. Pierron-Bohnes, C. Ulhaq-Bouillet, C. Pirri, M. H. Tuilier, D. Berling, P. Bertoncini, M. Gailhanou, and D. Thiaudière, Appl. Surf. Sci. **188**, 146 (2002).
[19] M. G. Proietti, H. Renevier, J.-L. Hodeau, J. Garcia, J.-F. Bérar, and P. Wolfers, Phys. Rev. B **59**, 5479 (1999).
[20] J. O. Cross, W. Tim Elam, J. C. Woicik, and L. B. Sorensen, J. Synchrotron Radiat. **6**, 335 (1999).
[21] M. Gailhanou, J. M. Dubuisson, M. Ribbens, L. Roussier, D. Bétaille, C. Créoff, M. Lemonnier, J. Denoyer, C. Bouillot, A. Jucha, A. Lena, M. Idir, M. Bessière, D. Thiaudière, L. Hennet, C. Landron, and J. P. Coutures, Nucl. Instrum. Methods Phys. Res. A **467-68**, 745 (2001).
[22] O. Ersen, C. Ulhaq-Bouillet, V. Pierron-Bohnes, M. H. Tuilier, D. Berling, P. Bertoncini, C. Pirri, M. Gailhanou, and D. Thiaudière, Appl. Phys. Lett. **81**, 2346 (2002).
[23] A. Michalowicz, J. Phys. IV **C2**, 235 (1997).
[24] S. Brenan and P. Cowan, Rev. Sci. Instrum. **63**, 850 (1992).
[25] D. T. Cromer and D. Libermann, Acta Crystallogr., Sect. A: Cryst. Phys., Diffr., Theor. Gen. Crystallogr. **37**, 267 (1981).
[26] M. Newville, B. Ravel, D. Haskel, J. J. Rehr, E. A. Stern, and Y. Yacoby, Physica B **208&209**, 154 (1995).
[27] S. I. Zabinsky, J. J. Rehr, A. Ankudinov, R. C. Albers, and M. J. Eller, Phys. Rev. B **52**, 2995 (1995).